ISTITUTO NAZIONALE DI ASTROFISICA
NATIONAL INSTITUTE FOR ASTROPHYSICS

ISTITUTO DI RADIOASTRONOMIA

Rapporto Interno n. 408/07

Report about the development of the proposal *"Sunyaev-Zel'dovich effect detection towards distant clusters"*

M.Zannoni, A.Tartari, M.Gervasi, G.Sironi
Dipartimento di Fisica "G. Occhialini" - University of Milano-Bicocca, Milano

V.Natale
INAF-IRA, Firenze

S.Molendi
INAF-IASF, Milano

1 Introduction

The main reason driving the development of this proposal is the need for the evaluation of the Noto antenna as a single-dish instrument for differential observations of weak cosmological signals at 40 GHz. In fact, when we are looking for the Sunyaev-Zel'dovich effect towards distant ($z \gtrsim 0.2$) clusters of galaxies at 40 GHz,

1. the beam of the telescope typically matches the core of the cluster, so we have no dilution, and

2. at this frequency the synchrotron emission, which is a contaminant, is suppressed by its power-law frequency dependence.

We add that the low system temperature of the receiver in principle allows a significant detection of the effect in few hours of observation, even with a narrow integration bandwidth. The observations were carried out between May 8 and May 12 2006; in the following the date is identified with the day number of the year.

Originally our targets were the clusters A773, whose SZ profile is well known at several frequencies, and RDCS 0949+4452 [1], but a technical problem forced us to postpone the observations at the beginning of May, while at the beginning they were planned between January and February 2006, so we timely considered to observe A2163 instead of RDCS 0949+4452. We observed A773 mainly during day-time (13-22 UT), while for A2163 we only collected night-time data.
During this campaign, which was thought to be a test to assess the feasibility of systematic SZ effect detections at 40 GHz, we observed the two clusters, Uranus, Saturn, Jupiter and other calibration sources (DR21, Tau A and Cas A) with two different observing schedules which we are going to describe.

2 Instrumental configuration

The reported data were obtained using the cryogenic dual circular polarization receiver for the 38 - 48 GHz band installed in the Noto antenna.

The receiver was tuned to the frequency of 43120 MHz. The data were collected over the total IF bandwidth, 400 MHz, of the VLBI terminal *MARKIV*. The noise temperature of the receiver is about 40K on both polarizations and the overall efficiency of the system is about 40% with the active surface correction enabled, dramatically decreasing to about 20% when the active surface is not enabled ([4]).

The observations were made using two observation modes: the beam switching (BS) by wobbling the subreflector and the position switching (PS) by moving the antenna. Because the observing efficiency is directly related to the implementation details of the observing mode, we briefly give a description of them.

The first one, BS implemented with the procedure SBEPL [3], is based on a beam switching at constant elevation with the lateral fields displaced $\sim 1'$ from the on-source

[1] The neighbouring regions of both clusters have been studied also in the framework the NRAO-VLA sky survey (NVSS). We used this survey to check the absence of radio sources in the lateral fields of our targets, in order to avoid undesirable off-sets in the differential measurements.

position. In this case, the time spent on each target position (On or Off-source) is 4 seconds (4 time constants of the integrator), while just one (the last) point is retained and is written on the data file. In this case, the beam switching is obtained moving the secondary mirror. Moreover the modulation can be performed not just when the antenna is pointing at the nominal source position, but also on two blank fields at the same right ascension as the target source, and displaced along the meridian by an amount $\Delta\delta = \pm 10'$. Consequently, running this schedule, either nine or three fields can be covered during each cycle, depending whether we observe Northern and Southern fields or not. Finally, we checked that the dead time between successive targets is negligible, so the *effective integration time* on-source is $\sim 12\%$ of the total observing time (T_{obs}), accounting for (1) 50% time spent off-source and (2) the 25% efficiency of SBEPL.

The second observing mode, PS implemented using the ad hoc procedure PSWITCH [3], is a position switch by moving the entire antenna. In this case the two lateral fields are displaced by $5'$ from the central position. The time spent on each target is 10 seconds, while the average value written on the data file is calculated on the last four records. In this case we only observe the source and the two lateral fields.
The question of dead time is more critical with PS, since the entire antenna is moving. In this case, 10 seconds are nominally spent on-target (On or Off fields), but there is a variable lapse of time between successive measurements, as we show in Figure 1, which refers to 4 hours of continuous observations of A2163 (day 133). From this data stream we assess an amount of dead time equal to 8% of the observing time. So the *effective integration time* spent on-source is $\sim 18\%$ of T_{obs}, accounting for (1) 50% time spent off-source, (2) dead time between targets and (3) 40% intrinsical efficiency of PSWITCH.

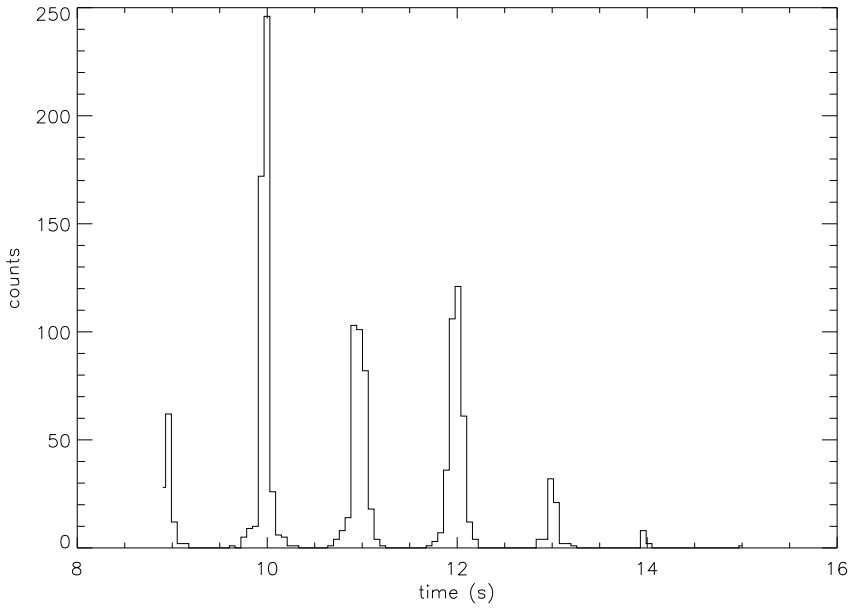

Figure 1: Time flowing between the beginning of measurements on successive targets.

Using both BS and PS among three fields, and calling W (West), E (East) and C (center) respectively the two off-source positions and the On-source position, a typical sequence of data is "$...C_W, W, C_E, E, C_W...$", where we have further labelled the two distinct central positions (C_E, C_W) in such a way that we can keep distinct the ONs followed by West or East lateral fields. This allows us to avoid a wrong estimate of the integration time and, consequently, a wrong statistical analysis. In this case, the source antenna temperature is

$$T_{source} = \frac{1}{2}[(T_{C_E} - T_E) + (T_{C_W} - T_W)]. \quad (1)$$

It is clear from this equation that we subtract the average of the two blank fields from the overall signal along the source's line of sight, with the underlying assumption that this quantity exactly represents the emission of the air-mass in the central field. Otherwise, an offset is expected. Moreover, the source temperature is measured in the two polarization channels, Tp1 and Tp2. The atmospherical optical depth have been measured several times every day during observations using the sky dip method, and its values are reported in Figure 2.

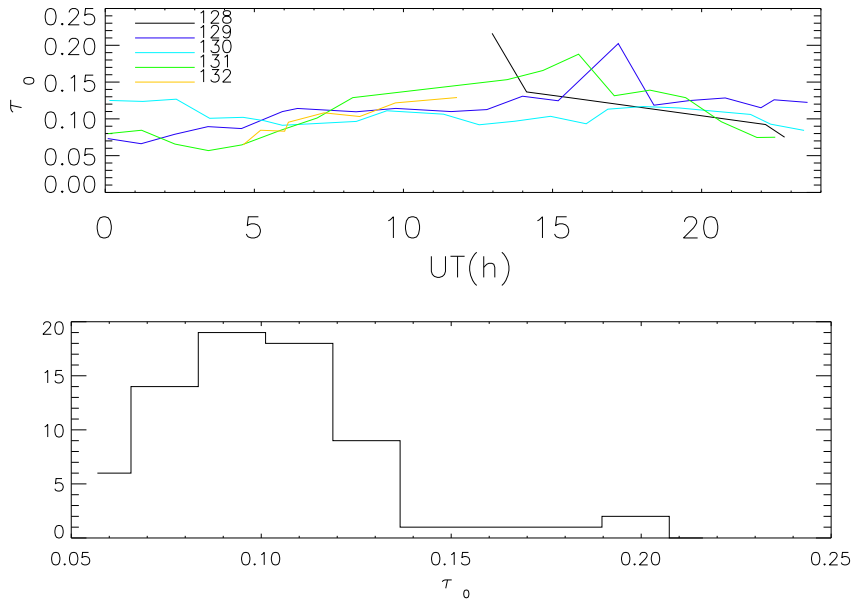

Figure 2: Top: the optical depth at $El = 90°$ during the observational campaign. The days are counted from the beginning of the year. Bottom: histogram of the same values as in the upper panel, representing the time sequence of the measurements.

3 Calibration

The antenna pointing performance, and the aperture efficiency were checked several times each day using the Field System procedure *FIVPT* using as sources both planets

and calibrators. In order to reconstruct the beam FWHM, the procedure uses scans along latitude and longitude till, after successive iterations, the beam in both directions is fitted with a centered Gaussian profile. The parameters we have extracted are the peak offset position (O_p), the FWHM of the beam and peak temperature, T_p. The results are collected in Table 1. In the last three columns of the table we also report: the observation elevation (EL); the atmospheric transmission ($e^{-\tau_0 cosec(EL)}$) with τ_0 derived by sky-dips; and the aperture efficiency η_a computed using the relation

$$\eta_a = \frac{2k_B}{SA_g}\kappa T_A \tag{2}$$

where S is the source flux density, A_g is the geometrical area of the antenna, k_B the Boltzmann constant, T_A the antenna temperature corrected for the atmospheric absorption, and κ a correction factor taking into account both the source and main beam profiles [1][2]. We adopted for the planets and calibrators the temperatures and the flux densities respectively published by Greve *et al.* [1].

Source	Day UT	*fit dir*	T_p(K)	O_p ($''$)	FWHM ($''$)	EL ($^\circ$)	$e^{-\tau}$	η_a ($\pm 3\sigma$)
Jupiter	128	*lat*	17.2 ± 0.2	13	63 ± 1	37	0.86	0.44 ± 0.01
	20:30	*lon*	17.2 ± 0.3	60	56 ± 1	37	0.86	0.44 ± 0.01
Jupiter	128	*lat*	20.7 ± 0.6	23	60 ± 2	30	0.80	$*$
	22:00	*lon*	21.6 ± 0.5	21	57 ± 2	30	0.80	$*$
Saturn	129	*lat*	2.5 ± 0.1	14	68 ± 4	72	0.84	$*$
	16:00	*lon*	3.3 ± 0.3	94	37 ± 5	72	0.84	$*$
DR21	129	*lat*	1.04 ± 0.01	37	53 ± 1	73	0.89	0.26 ± 0.01
	06:00	*lon*	1.02 ± 0.01	12	61 ± 1	73	0.89	0.25 ± 0.01
DR21	129	*lat*	1.22 ± 0.05	35	53 ± 2	67	0.88	0.31 ± 0.02
	06:30	*lon*	1.14 ± 0.03	2	57 ± 2	67	0.88	0.29 ± 0.01
DR21	129	*lat*	1.24 ± 0.02	35	53 ± 1	45	0.86	0.32 ± 0.01
	08:30	*lon*	1.30 ± 0.04	6	55 ± 2	45	0.86	0.33 ± 0.01
DR21	129	*lat*	1.33 ± 0.08	6	78 ± 7	32	0.81	0.36 ± 0.02
	09:45	*lon*	0.9 ± 0.1	2	62 ± 9	32	0.81	0.25 ± 0.03

Table 1: Planets and calibrators observed with the *FIVPT* procedure

In particular for Jupiter, using their flux density, we obtain $\eta_a = 0.44 \pm 0.01$ (3σ), in good agreement with the expected performances of the telescope [4]. We cannot follow a similar way with *FIVPT* Saturn data, because the closest sky-dips have been done one hour before and one hour after running *FIVPT*, but in the meanwhile the values of τ_0 have changed considerably, i.e. from 0.12 to 0.22 (in the table, we assumed a mean value of 0.17 for the calculation of the transmission). Unavoidably the efficiency derived in this way would be unreliable.

The most reliable value of Saturn's antenna temperature outside atmosphere is therefore $(3.31 \pm 0.01)K$ obtained tracking the source with SBEPL (beam-switching,

[2]If the source is considered to be a uniform disk of diameter θ_D and observed with a Gaussian beam with FWHM θ_B, defining $x = \sqrt{ln2}\theta_D/\theta_B$, then $\kappa = x^2/[1 - exp(-x^2)]$[2]. Its values for Jupiter, DR21, Saturn and Uranus are respectively 1.213, 1.048, 1.031 and 1.002. In the case of DR21 we should consider a Gaussian brightness profile with $\kappa = 1.137$.

see paragraph 5 for details). With the flux density reported in [1], we can assess $\eta_a = 0.31 \pm 0.01$ at 3σ level. In the same way, we obtain $\eta_a = 0.13 \pm 0.06$ from Uranus (not reported in Table 1 since this source was too weak to be observed with *FIVPT* schedule).

Observing Saturn and Uranus by means of PS or BS, a pointing error during tracking (possibly worsened due to the loss of synchronization between the clock and the pointing system) unavoidably translates in a lower antenna temperature and consequently in a wrong estimate of the aperture efficiency η_a. In the case of Uranus, we could invoke a pointing error of $30''$ to account for the low value of antenna temperature.

The conclusion which seems more appropriate is that the efficiency with the active corrections at work sets correctly around 40%.

The values of the beam (FWHM) always lie between $53''$ and $63''$ (with the exception of the values obtained scanning across Saturn).

We add a last remark concerning the pointing accuracy. As we can see in Figure 3, where DR21 observations with *FIVPT* are shown, the pointing accuracy is not trivially related to the elevation. In particular, the pointing offsets are greater along the latitude direction. We do not know if this anomalous behavior can be ascribed to a bad performance of the active surface of the telescope or not.

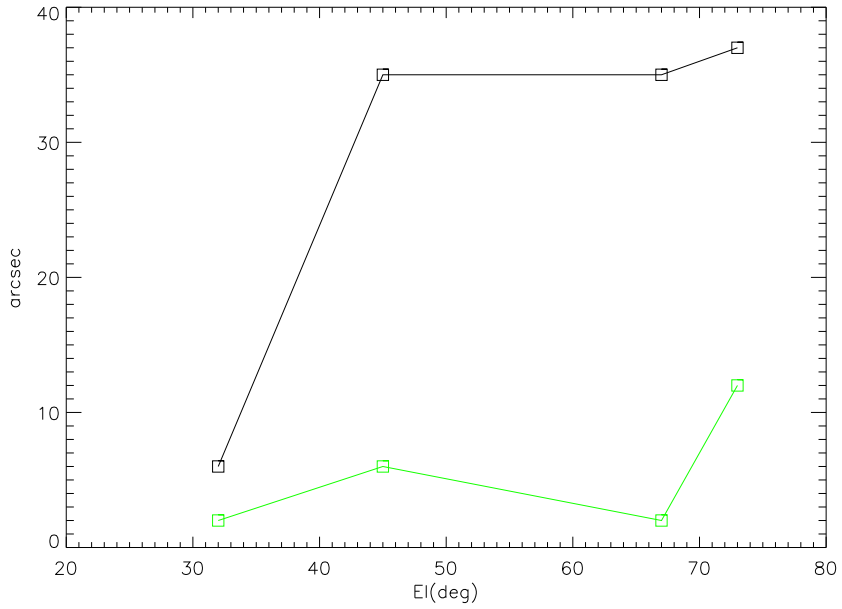

Figure 3: DR21 observed with *FIVPT*. The peak power offset $O_p('')$ *vs* elevation (°). Green squares: scans along longitude. Black squares: scans along latitude.

3.1 Performance of the observing modes

Both the modulation efficiency and the offset level and stability are of fundamental importance in programming weak signal observations.

A fundamental issue which we try to address in few lines is the offset due to an incomplete cancellation of the lateral blank fields. Obviously this is a fundamental problem for differential techniques because it is a source of systematic errors and can hamper the detection of a weak signal regardless of the integration time. Unfortunately this effect has been observed unequivocally three times using SBEPL: once on a blank field at $\delta = 60°$; then observing Uranus and Saturn with their northern and southern blank fields.

At the beginning of the campaign, during the first day of observations (128), we observed two blank fields, namely [$\alpha = 00^h00^m00^s$, $\delta = 30°00'00''$] and [$\alpha = 00^h00^m00^s$, $\delta = 60°00'00''$] in order to check the offset level and stability using BS. The first region, with its northern and southern fields, has only been observed for 27 minutes with SBEPL, while the sky was covered by clouds. As we can see in Figure 4, the data are quite noisy and only the last block of data sets around an almost flat level near the null signal. The second one has been observed for a longer time, 87 minutes, and this time only the central blank field has been modulated. In this case we have found a non null (differential) signal, according to equation 1, both for Tp1 and Tp2, whose values are respectively -13 and -12 mK with 2 mK statistical error bar.

The values obtained from the blank fields at the north and south of the nominal position of Uranus and Saturn are respectively $T^N_{Uranus} = (-42 \pm 7)mK$, $T^S_{Uranus} = (-39 \pm 7)mK$, $T^N_{Saturn} = (-12 \pm 4)mK$ and $T^S_{Saturn} = (-11 \pm 5)mK$. For completeness, we recall that the blank field has been observed in a elevation range $69° \div 82°$, while Saturn has been observed for a short time when it was around $El = 72°$. Uranus, whose measurement seems to be conditioned by a greater offset, has been observed when its elevation was in the range $31° \div 45°$. Lacking other observations of this kind on known sources, the correlation between offset and elevation remains a guess which needs urgently to be confirmed or discarded.

4 DR21, Tau A and Cas A

Here and in the following paragraphs we will quote the antenna temperature of the source outside atmosphere, that is $T_A = T^*_A e^{\tau_0 cosec(El)}$, where El is the elevation angle, τ_0 is the optical depth at $El = 90°$ and T^*_A is the value measured with the $K/counts$ conversion factor obtained injecting the noise mark.

Both Tau A and Cas A have been observed only with PSWITCH due to their angular extent, pointing at their nominal center. The results are:

- $T_{TauA} = (2.37 \pm 0.01)K$, with a non detectable East-West asymmetry in blank fields;
- $T_{CasA} = (0.675 \pm 0.005)K$, even if in this case we measure $T_{E-W} = (0.03 \pm 0.01)K$, so the error can be realistically raised to the second significant figure.

DR21 has been observed both with PSWITCH and SBEPL. The antenna temperatures of the source obtained with these two techniques are respectively $(1.12 \pm 0.01)K$ and $(1.16 \pm 0.03)K$. In both cases they are well below the peak temperatures recorded with *FIVPT* ($\sim$ 1.6K) and, if we believe these values, we should also conclude that $\eta_a = 0.25 \div 0.26$ (assuming that the brightness distribution of the source is Gaussian).

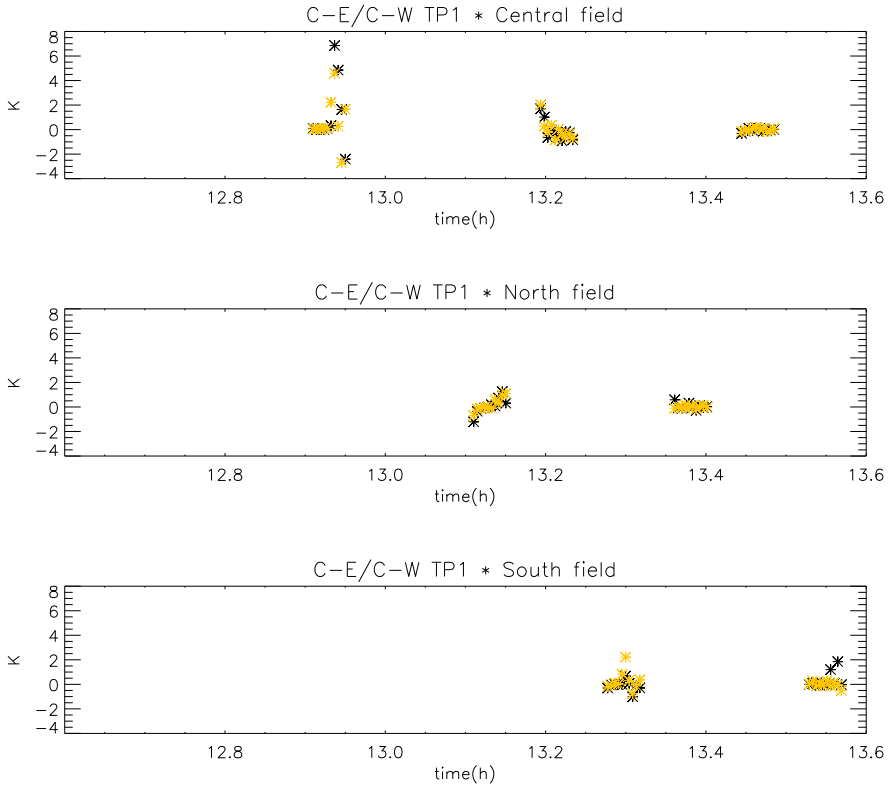

Figure 4: A blank field at $\alpha = 00^h00^m00^s$, $\delta = 30°00'00''$, and its northern and southern fields. The differential signals, $T_{C_E} - T_E$ and $T_{C_W} - T_W$, are plotted *vs* UT time for the channel Tp1 only.

5 Planets

5.1 Uranus

Uranus has been observed with PS during the day 129.
For each polarization channel we obtained 45 measurements of T_{source} (see Equation 1), each differential measurement requiring 16 seconds. The optical depth of the atmosphere has been measured before and after the observation of the planet. We have found $\tau_0 = 0.110$ and $\tau_0 = 0.114$ respectively, so that we adopted the mean value for the atmospheric correction. We found $T_{Uranus} = (75 \pm 9)mK$. We also observed that on average the difference between the lateral fields is $T_{E-W} = (-30 \pm 10)mK$, which has to be considered a systematic effect.

Three schedules have been planned to observe Uranus with a beam-switching (BS) technique. The first one has been written for the day 130, when we didn't plan to observe the North and South fields (at $\Delta\delta = \pm 10'$). On the contrary, we did for other two schedules, planned to be run on days 131 and 132. The temperature measured using the first schedule was $T_{Uranus} = (86 \pm 5)mK$, with a difference between the

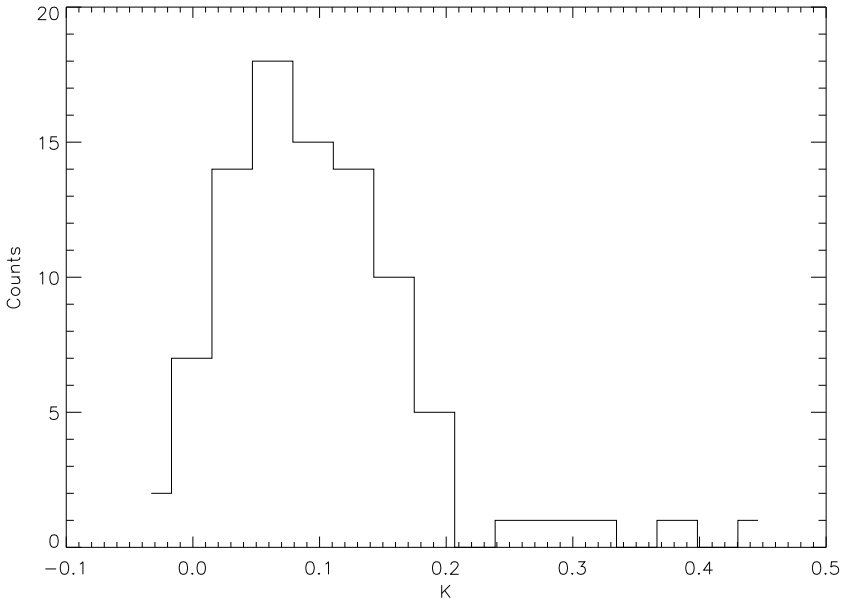

Figure 5: Uranus. Tp1 and Tp2 are shown jointly in a single histogram.

lateral fields well inside the statistical error bar, that is $T_{E-W} \leqslant 8mK$.

From the second schedule we obtained the temperature of the source as well the temperature of the North and South blank fields. These are the results: $T_{Uranus} = (48 \pm 7)mK$; $T_{\Delta\delta=+10'} = (-42 \pm 7)mK$; $T_{\Delta\delta=-10'} = (-39 \pm 7)mK$. If we correct the value of the source's temperature subtracting the average value of the reference (blank) fields, we can state that the temperature of the planet is $(88 \pm 10)mK$.

During the running of third schedule no source has been detected, probably due to a pointing error.

The discrepancy among the results shown in this section, could be ascribed to many reasons. Here we can only list some of them: a residual atmospheric contribution due to fluctuations faster than the modulation frequency, a too wide modulation amplitude, a beam deformation when the secondary mirror is tilted off-axis.

5.2 Saturn

The value obtained for Saturn using PS is $T_{Saturn} = (2.74 \pm 0.06)K$, and in this case we have found also $T_{E-W} = (0.6 \pm 0.1)K$, but such an important effect could be due partially to the motion of the planet with respect to the celestial sphere and to the consequent "migration" of the planet towards one of the two OFF-source fields. Another fact to be pointed out is that during the observations of Saturn (but the same situation has been observed also in the case of DR21), we noticed that the clock and the computer controlling the pointing of the antenna sometimes were not synchronized and, as soon as synchronization was restored restarting the system, the on-source celestial signal increased dramatically. In fact, on Saturn, the temperature measured during the position switch, just before re-synchronization, was $(0.99 \pm 0.07)K$ (to be

compared with the value previously given).

Two BS schedules including the observation of the northern and southern fields have been run during the days 128 and 129. We summarize the results concerning the observations of Saturn in Tab. 2.

day	T_{Sat}(K)	T_N(K)	T_S(K)
128	2.89 ± 0.02	-0.020 ± 0.005	-0.011 ± 0.007
129	3.30 ± 0.01	-0.012 ± 0.004	-0.011 ± 0.005
day	T_{Sat}^{E-W}(K)	T_N^{E-W}(K)	T_S^{E-W}(K)
128	0.29 ± 0.02	0.03 ± 0.01	0.04 ± 0.01
129	0.22 ± 0.01	0.03 ± 0.01	0.04 ± 0.01

Table 2: Saturn: beam switching

Two remarks are worth attempting.

1. If one defines a reference temperature as the average of the two blank fields, it's possible to obtain values of the planet's temperature corrected for the offset. Referring to the first and to the second day of observations, we found respectively:

   • the offset temperatures $T_{off} = (-0.016 \pm 0.006)K$ and $T_{off} = (-0.011 \pm 0.005)K$;

   • the corresponding corrected planet's temperatures $T_{Sat,cor} = (2.91 \pm 0.03)K$ and $T_{Sat,cor} = (3.31 \pm 0.02)K$. The quoted error bars have to be intended as statistical uncertainties and since the measurements made on two subsequent days are completely incompatible (they differs of more than 10 σ), we can can consider them as a proof of not understood systematic effect.

2. The "unbalancing" between the East-West fields is stronger in correspondence of the planet ($\Delta\delta = 0'$), so that it's likely that it's due to the motion of the planet respect to the celestial sphere. In fact, when using SBEPL, the three fields at constant elevation are separated by just one beam (so they're even closer than during a position switch.)

We underline that the problem of clock's synchronization has been observed in the morning of day 129, so that it's likely that the discrepancy among the value of Saturn's antenna temperature recorded during these two days is ascribable to a drift in pointing accuracy.

5.3 Jupiter

Jupiter has been observed only once with SBEPL, in fact we noticed that we were loosing rapidly the correct pointing of the source, so that we decided not to track it anymore. This can be stated looking at the first panel in Fig.6, where it is possible to notice a strong asymmetry between the C-E and C-W signals, which becomes even stronger as the time flows. Conversely, this asymmetry disappears in the North ($\Delta\delta = +10'$) and South ($\Delta\delta = -10'$) blank fields. In the last sequence of records even the $T_{C_W} - T_W$ becomes negative, meaning that the planet is predominantly observed in a lateral field.

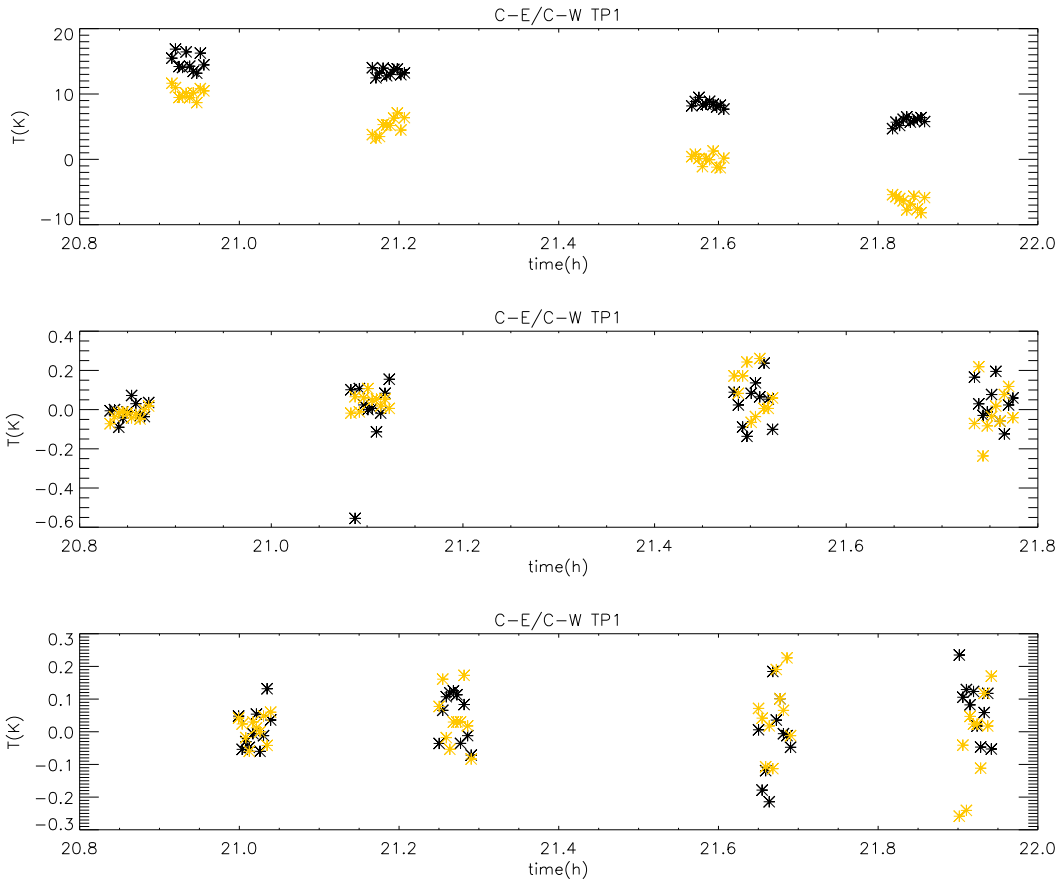

Figure 6: Jupiter. In the three panel are shown respectively the source and the North and South blank fields. The colors refer to the differences $T_{C_E} - T_E$ and $T_{C_W} - T_W$. Clearly the planet is moving among the three fields at constant elevation.

6 Observations of A773 and A2163

6.1 Observations with Position Switch

The data stream is a sequence $\{S_n\}$ of on and off-source measurements. Since the sky signal is modulated among three fields, and the n-*th* element of the vector D containing the difference between adjacent fields is

$$D_n = \frac{1}{2}[1 + (-1)^n][(-1)^n S_n + (-1)^{n+1} S_{n+1}], \tag{3}$$

or, rearranging this expression to show explicitly the de-modulating waveform,

$$D_n = \frac{1}{2}\{S_n[1 + (-1)^n] + S_{n+1}[(-1)^{n+1} + (-1)^{2n+1}]\}, \tag{4}$$

it's easy to show that the odd-indexed components of the vector D are null, while the even-indexed components are stored in a vector $\bar{D} = \{D_{2n}\}$. In Figure 7, we show the vector $\bar{D}$ built for both Tp1 and Tp2 during the observations of A2163 (day 133). In

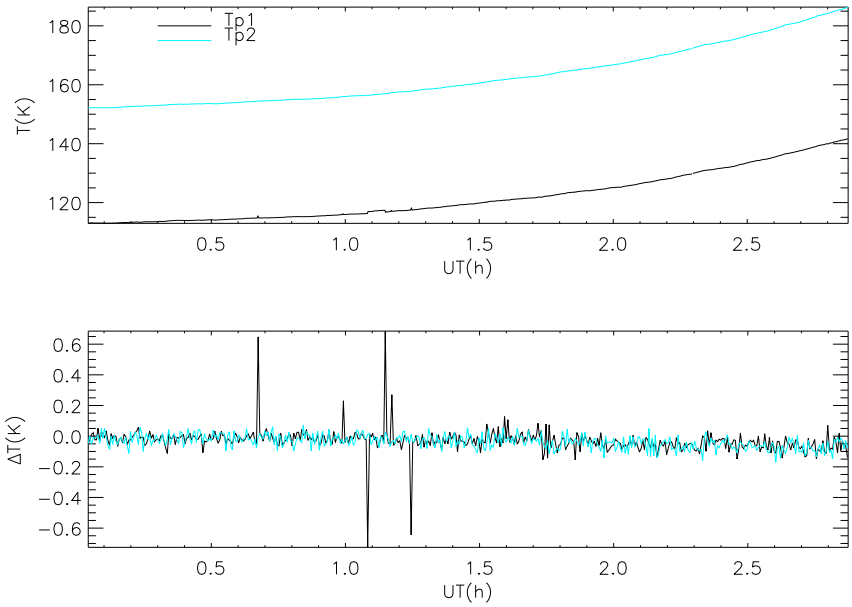

Figure 7: Day 133. Observation of A2163 using PSWITCH. Upper panel: the total power signal Tp1 and Tp2. Lower panel: differential signal after demodulation for both channels.

the same picture (upper panel), we show the total power signal before demodulation: it is possible to observe the drift, due to the change in elevation, and the effectiveness of the modulation-demodulation process. It is also possible to check that, neglecting dead times, we need 20 seconds to built one element of the D-vector and 40 seconds for the $\bar{D}-$vector.

Then we can evaluate the minimum variance by means of the Allan plot, that is the variance *vs* the integration time, knowing that the integration time Δt is a fraction ($\sim 18\%$) of the observational time. In the Fig.8 and 9 we plot the calculated two-sample variance (omitting the factor 1/2) of $\bar{D}$ *vs* Δt. Due to the fact that data records are not always evenly spaced, these plots could be affected by artifacts and they cannot be used to obtain detailed noise spectral features. Nevertheless they can be used to get some hints about the useful range of integration time determined by the regions in which the Allan plot starts to flatten: see for example the upper-left panel in Fig.8 or the third panel in Fig.9. In the cases in which the variance no longer decreases increasing the integration time, the limiting integration time has been reached and the ultimate statistical sensitivity with it. Anyway this turning point is not evident in all the plots shown in Fig.8 and Fig.9. We can conclude that the minimum variance reached in every sequence, except the A773-132 (third) sequence, is of the order of $10^{-4}K2$ for integration of few hundreds of seconds in both polarizations. We would stress that these limits barely suggest how an observing session can be subdivided into shorter (and continuous) time intervals by means of the insertion of calibration procedures, and how long these intervals could be. The final conclusion of this analysis is that during these observations there has been an excess of low frequency noise due both

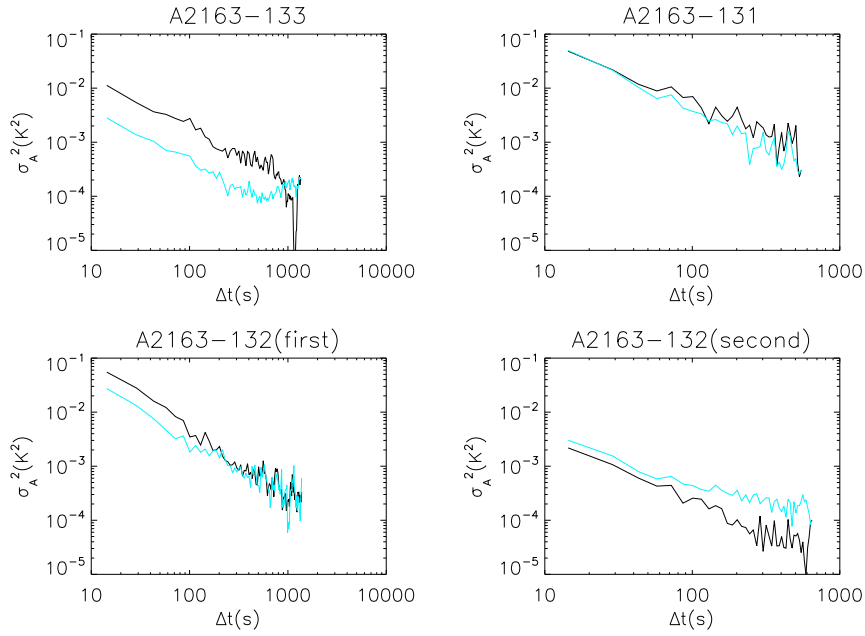

Figure 8: A2163. The Allan variance of the $\bar{D}$ vector during different days. In abscissa the effective integration time.

to atmospheric instabilities and, may be, to the receiving system; consequentely the estimate of sensitivity, relying on the assumption of white noise, is misleading. In fact, with a careless application of the *radiometer equation* we would obtain unreasonably high values of the system temperature ($\sim 3000K$). The same result can be obtained looking at Figure 10, where we show all the data collected during the observation of A773 against the background: here the sample standard deviation is 86 mK for an equivalent integration time of about 10 sec.

6.2 Observations with Beam Switching modulation

6.2.1 Raw data

Data collected with the SBEPL procedure are a sequence of signals coming from the nominal source and two reference fields one beam apart in east and west directions. It is a classical three-fields modulation which should be particularly effective when looking for signals like SZ which are brightness decrements with respect to the undisturbed CMB flux density. In particular, the data collected are centered on the cluster and on two reference fields whose declinations are $\pm 10'$ with respect to the cluster's one. In such a way a rectangular grid like the one in Figure 11 is sampled.

The reason to collect data from the two reference fields is to correct for possible offsets induced by the modulation of the telescope secondary mirror. If the two reference fields (north and south) are actually *"blank"* fields, i.e. no SZ signal is present, a non-null difference between the central and lateral fields can be ascribed to an offset (see later in Section 6.2.3).

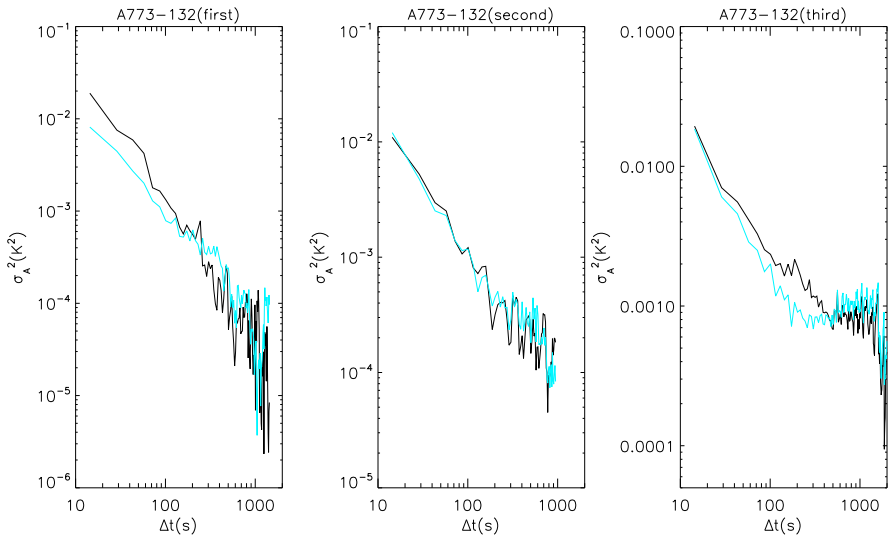

Figure 9: A773. Allan plot. see comments in the caption of Fig. 8.

At the beginning of each sequence the receiver was calibrated in both polarizations. First of all, the ADC offset is evaluated, then data to compute the Kelvin/Counts conversion factor are collected by observing a nominally blank field with and without a calibration signal.

6.2.2 Demodulation, Calibration and Atmospheric Correction

Demodulation is performed in the same way as for equation 4. For each pointing (Cluster, Reference North, Reference South) and for each polarization, the two differences $Centre - East$ and $Centre - West$ are computed. The data are then converted into Temperature and corrected for atmospheric absorption with the nearest evaluation of τ. To obtain the SZ signal each successive difference $Centre - East$ and $Centre - West$ is averaged ($\frac{1}{2}[(C-E)+(C-W)]$). The next step is to correct for offset.

6.2.3 Offset correction

Offset is taken into account in the following way. Consider the differences $C - E$ and $C - W$. They can be rewritten as

$$\begin{aligned} (C-E)^{obs} &= (C-E)^{real} + OS^{C-E} \\ (C-W)^{obs} &= (C-W)^{real} + OS^{C-W} \end{aligned} \tag{5}$$

in order to take into account for different offset (OS) generation when moving the secondary mirror to observe the lateral fields. The same thing can be done on the northern and southern fields where, under the assumption they are *blank fields*, the

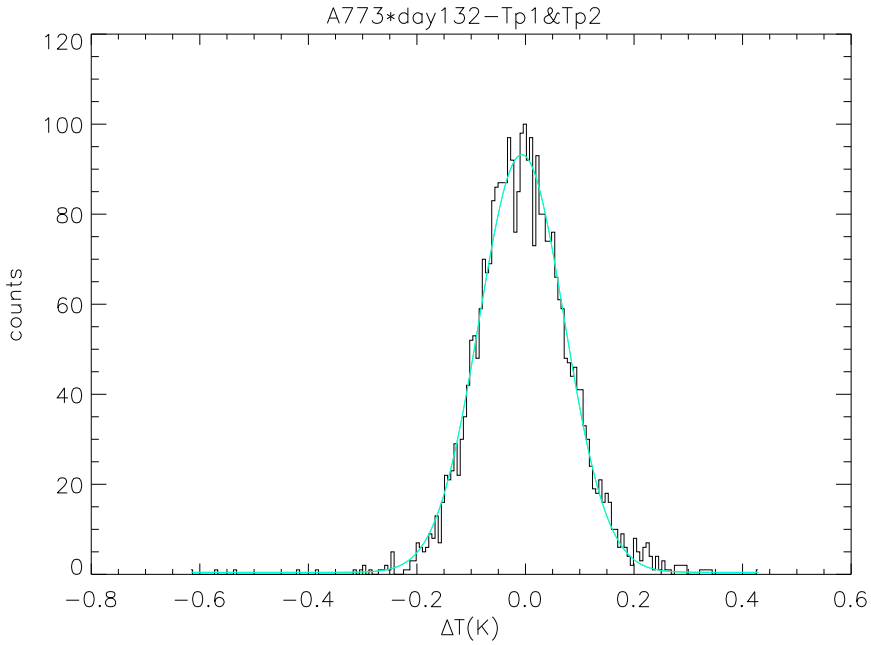

Figure 10: A773 observed during the day 132 using PSWITCH. Number of counts *vs* the value of the differential signal (in K). All the data obtained in about 8 hours of observation and in both polarizations are reported on the same plot.

non-null difference is a genuine measure of the offset, even if in a slightly different configuration (the antenna is pointing at a declination $\pm 10'$ with respect to the cluster position). So we can write

$$\begin{aligned} (C-E)^N &= OS^{N-E} \\ (C-W)^N &= OS^{N-W} \\ (C-E)^S &= OS^{S-E} \\ (C-W)^S &= OS^{S-W}. \end{aligned} \tag{6}$$

This allows us to evaluate the offset generation in the cluster field as

$$\begin{aligned} OS^{C-E} &= \frac{1}{2}(OS^{N-E} + OS^{S-E}) \\ OS^{C-W} &= \frac{1}{2}(OS^{N-W} + OS^{S-W}). \end{aligned} \tag{7}$$

Now the SZ signal evaluated as $\frac{1}{2}[(C-E)+(C-W)]$ can be written in the light of the previous expressions

$$\frac{1}{2}[(C-E)^{obs} + (C-W)^{obs}] = \frac{1}{2}[(C-E)+(C-W)] + \frac{1}{2}[OS^{C-E} + OS^{C-W}]. \tag{8}$$

With some trivial algebra we can find

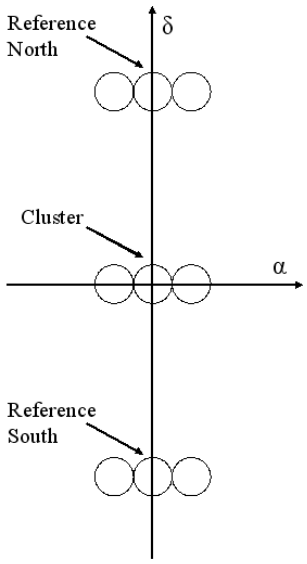

Figure 11: The grid sampled in the sky by means of SBEPL technique. In RA direction the fields are separated by 1 beam (54"), in DEC by 5'.

$$\frac{1}{2}[(C-E)^{obs}+(C-W)^{obs}] = \frac{1}{2}[(C-E)+(C-W)]+\frac{1}{2}\{\frac{1}{2}[OS^{N-E}+OS^{S-E}]+\frac{1}{2}[OS^{N-W}+OS^{S-W}]\}. \tag{9}$$

Now we can write

$$\frac{1}{2}[(C-E)+(C-W)] = \frac{1}{2}[(C-E)^{obs}+(C-W)^{obs}] - \frac{1}{2}[OS^{N}+OS^{S}], \tag{10}$$

where we have indicated

$$\begin{aligned} OS^{N} &= \frac{1}{2}(OS^{N-E}+OS^{N-W}) \\ OS^{S} &= \frac{1}{2}(OS^{S-E}+OS^{S-W}). \end{aligned} \tag{11}$$

The results of the analysis of the three different days of observation of the two clusters A773 and A2163 are summarized in Tab.3.

In Tab. 3 the last column reports the SZ data corrected for every disturbing effect (ADC offset, atmospheric transparency, modulation-driven offset). It is evident that they are all compatible with zero, with the only exception of A773, day 11^{th} of May, second polarization, which shows a $\Delta T_{SZ} = -0.010 \pm 0.003K$. Apparently a marginal detection, $\Delta T_{SZ} = -0.013 \pm 0.009K$, is present in the last day for A2163 too. However we can be confident that these results aren't real detections for the following reasons. First of all, where we have a possible detection, in both polarization the signal is compatible with zero. Secondly, the A773 signal is too high with respect to the one

Day	Cluster	North	Center	South	OffSet	SZ
05/09/2006	A773	-0.034 ± 0.007 -0.018 ± 0.008	-0.016 ± 0.004 -0.023 ± 0.004	-0.007 ± 0.004 -0.006 ± 0.005	-0.020 ± 0.008 -0.012 ± 0.009	0.004 ± 0.009 -0.011 ± 0.009
05/10/2006	A773	-0.011 ± 0.002 -0.008 ± 0.002	-0.009 ± 0.002 -0.011 ± 0.002	-0.010 ± 0.002 -0.005 ± 0.002	-0.010 ± 0.003 -0.013 ± 0.003	0.0005 ± 0.004 0.001 ± 0.004
05/11/2006	A773	-0.0006 ± 0.003 -0.004 ± 0.004	-0.004 ± 0.0034 -0.010 ± 0.003	0.001 ± 0.004 0.005 ± 0.004	0.0002 ± 0.005 0.0005 ± 0.006	-0.004 ± 0.003 -0.010 ± 0.003
05/08-09/2006	A2163	-0.006 ± 0.005 -0.003 ± 0.005	-0.0005 ± 0.004 -0.0009 ± 0.005	-0.009 ± 0.004 -0.002 ± 0.006	-0.0075 ± 0.004 -0.0025 ± 0.008	0.007 ± 0.007 0.002 ± 0.009
05/09-10/2006	A2163	0.005 ± 0.005 0.010 ± 0.005	0.008 ± 0.004 0.014 ± 0.004	0.007 ± 0.004 0.002 ± 0.004	0.0085 ± 0.006 0.006 ± 0.006	-0.0005 ± 0.006 0.008 ± 0.007
05/10-11/2006	A2163	0.017 ± 0.005 0.017 ± 0.005	0.008 ± 0.005 0.005 ± 0.005	0.018 ± 0.005 0.020 ± 0.005	0.0175 ± 0.007 0.0185 ± 0.007	-0.009 ± 0.009 -0.013 ± 0.009

Table 3: The results of the analysis on the cluster data for every day of observation. Each cell reports the values in Kelvin for both polarizations.

Pol	A773	A2163
TP1	-0.002 ± 0.002	0.0003 ± 0.004
TP2	-0.006 ± 0.002	0.0006 ± 0.005

Table 4: Weighted average of SZ signals.

already detected by the Nobeyama team ($\sim 1mK$ [5]) chiefly if we take into account that our modulation width is so tight (less than 1') that the estimated decrement shouldn't exceed $0.3 - 0.4mK$. The weighted averages, reported in Table 4, of the SZ signals confirm this conclusion.

We think that the main reason for the failure of SZ detection comes out from the following difficulties:

- uncorrect offset cancellation, possibly due to different levels of stray-light contamination (in fact, for example, it is known that the offset emerging from blank fields changes with the elevation, see 3.1 and [3]);
- pointing accuracy: the varying pointing offset translates into a wrong SZ decrement measurement due to the fact that the cluster's core can be out of the main beam and, moreover is not a random effect, but it's probably elevation-dependent;
- observational strategy which is not suitable to exploit the receiver performance in its white-noise-dominated regime.

7 Conclusions

The main conclusion to be drawn from the data analysis, is that we have not detected the Sunyaev-Zel'dovich effect in A772 and A2163, neither with position-switching, nor with beam-switching techniques. Nevertheless, this campaign has clearly pointed out some problems (see 6) that realistically hamper the detection of weak cosmological signals using differential techniques. We won't repeat the considerations done in the previous section, but it's worth underlining that one of the main issues to be faced (in view of future similar campaigns) is the choice of a proper observational strategy which (1) should allow a greater time efficiency, (2) should be less prone to systematics and (3) should be able to exploit the receiver's performance near its white noise floor. In sight of future campaigns, we suggest a systematic study of the beam shape when the secondary mirror in the off-set positions and the check of the active surface effectiveness. The synchronization of the clock must be fixed, otherwise the pointing accuracy is rapidly lost. It will also be very useful to develop a back-end independent from the VLBI Field System with a faster sampling rate useful for OTF observations and for a fast injection of the noise mark to keep $1/f$ noise under control.

Acknowledgements

We acknowledge Paolo Leto, Corrado Trigilio and Giuseppe Maccaferri for helping us during the planning and the development of the observational campaign. We also acknowledge the Noto VLBI station technical staff for the warm hospitality.

References

[1] Greve, A., *et al.*, 1994, *A& A*, **286**, 654-658

[2] Gordon, M.A., *et al.*, 1992, *A& A*, **264**, 337-344

[3] Leto, P., 2006, *private communication*

[4] Bolli, P., *et al.*, 2003, I.R.A. Internal Report N.332/03

[5] Tsuboi, M., *et al.*, 2004, **PASJ: 56**, 711-721